Proc. Natl. Acad. Sci. USA
Vol. 92, pp. 7789–7793, August 1995
Biophysics

Light-generated nuclear quantum beats: A signature of photosynthesis

STEFAN WEBER†, ERNST OHMES†, MARION C. THURNAUER‡, JAMES R. NORRIS‡, AND GERD KOTHE†§

†Department of Physical Chemistry, University of Stuttgart, Pfaffenwaldring 55, D-70569 Stuttgart, Germany; and ‡Chemistry Division, Argonne National Laboratory, Argonne, IL 60439

Communicated by S. I. Weissman, Washington University, St. Louis, MO, May 8, 1995 (received for review August 15, 1994)

ABSTRACT **Light-induced radical pairs in deuterated and deuterated plus ^{15}N-substituted *Synechococcus lividus* cyanobacteria have been studied by transient EPR following pulsed laser excitation. Nuclear quantum beats are observed in the transverse electron magnetization at lower temperatures. Model calculations for the time profiles, evaluated at the high-field emissive maximum of the spectrum, indicate assignment of these coherences to nitrogen nuclei in the primary donor. Thorough investigation of the nuclear modulation patterns can provide detailed information on the electronic structure of the primary donor, providing insight into the mechanism of the primary events of plant photosynthesis.**

Spin-correlated radical pairs (1–7) are generated as short-lived intermediates in the primary energy conversion steps of natural photosynthesis (1, 5–14). If the initial configuration of the radical pair is not an eigenstate of the corresponding spin Hamiltonian, the radical pair starts out in a coherent superposition of spin states (15–19), which can manifest itself as *quantum beats* in an EPR experiment with adequate time resolution (20–24). In the following we report transient EPR studies of light-induced radical pairs in plant photosystem I (PSI) with particular reference to *nuclear spin coherences* generated by a laser pulse.

The primary electron transfer process in PSI involves the primary chlorophyll donor P_{700} and a series of protein-bound acceptors, A_0, A_1, F_X, F_A, and F_B (25). Although the PSI reaction center has been crystallized, its x-ray structure is not known with great detail (26). Yet there is substantial evidence that two chlorophyll molecules, the special pair (27), form the primary donor (26, 28). Furthermore, current evidence suggests that A_0 is a chlorophyll species and F_X, F_A, and F_B are iron–sulfur (FeS) centers. A_1 has been identified as vitamin K_1 (29). Thus, existing information points to the following chain of electron transfer steps, initiated by photoexcitation of the donor P_{700} (25, 29):

$$P^*_{700}A_0A_1(FeS) \rightarrow P^+_{700}A_0^-A_1(FeS)$$

$$\rightarrow P^+_{700}A_0A_1^-(FeS) \rightarrow P^+_{700}A_0A_1(FeS)^-.$$

A light-induced EPR signal with characteristic e/a/e polarization (e = emissive, a = absorptive) was observed in PSI a number of years ago (30, 31). Yet the identity of this signal remained unclear. Recent work proves a direct assignment of the polarized spectrum to the secondary radical pair, $P^+_{700}A_1^-$ (29, 32). Here we report observation of *nuclear quantum beats* for $P^+_{700}A_1^-$ in deuterated and deuterated plus ^{15}N-substituted *Synechococcus lividus* cyanobacteria and suggest how these coherences may be used to obtain structural details of the primary donor P^+_{700}.

The publication costs of this article were defrayed in part by page charge payment. This article must therefore be hereby marked "*advertisement*" in accordance with 18 U.S.C. §1734 solely to indicate this fact.

THEORY

In this section we briefly summarize a model for transient EPR of spin-correlated radical pairs and define the model parameters (16, 21–23). Specifically, we consider a sudden light-induced generation of the radical pair with a spatially fixed geometry. Particular emphasis is given to the nuclear spin interactions, essential for the modeling of nuclear quantum beats.

The total spin Hamiltonian, $H(\Omega, t)$, depends on the orientation, Ω, of the radical pair and can be divided into seven parts:

$$H(\Omega, t) = H_Z(\Omega) + H_R(\Omega, t) + H_{EX} + H_D(\Omega) + H_{HF}(\Omega) + H_{NZ} + H_Q(\Omega). \quad [1]$$

The first term, describing Zeeman interactions of the electron spins $\mathbf{S}_i$, $i = 1, 2$, with the static magnetic field $\mathbf{B}_0 = (0, 0, B_0)$ is given by

$$H_Z(\Omega) = \beta\mathbf{B}_0\cdot[\mathbf{g}_1(\Omega)\cdot\mathbf{S}_1 + \mathbf{g}_2(\Omega)\cdot\mathbf{S}_2], \quad [2]$$

where β and $\mathbf{g}_i$, $i = 1, 2$, are the Bohr magneton and the g-tensor of radical i, respectively.

In the presence of a rotating microwave field $\mathbf{B}_1 = (B_1\cos\omega t, B_1\sin\omega t, 0)$ the Hamiltonian includes the radiation term,

$$H_R(\Omega, t) = \beta\mathbf{B}_1\cdot[\mathbf{g}_1(\Omega)\cdot\mathbf{S}_1 + \mathbf{g}_2(\Omega)\cdot\mathbf{S}_2], \quad [3]$$

where B_1 denotes the magnitude of the microwave radiation. The next two terms of Eq. **1** account for the isotropic and anisotropic spin–spin coupling of the radical pair,

$$H_{EX} = J(Q_T - Q_S), \quad [4a]$$

$$H_D = (\mathbf{S}_1 + \mathbf{S}_2)\cdot\mathbf{D}(\Omega)\cdot(\mathbf{S}_1 + \mathbf{S}_2), \quad [4b]$$

$$Q_T = \left(\frac{3}{4} + \mathbf{S}_1\cdot\mathbf{S}_2\right), \quad [4c]$$

$$Q_S = \left(\frac{1}{4} - \mathbf{S}_1\cdot\mathbf{S}_2\right), \quad [4d]$$

where J and $\mathbf{D}(\Omega)$ are the electron exchange interaction and the dipolar coupling tensor, respectively. Since $\mathbf{D}(\Omega)$ is traceless, two zero-field splitting parameters, D and E, suffice to specify the diagonal tensor.

The fifth term of the Hamiltonian **1** describes the magnetic interactions between electron and nuclear spins. For weakly coupled radical pairs this part of the Hamiltonian can be written as (33)

Abbreviations: PSI, plant photosystem I; Nd:YAG, neodymium-doped yttrium–aluminum garnet; ENDOR, electron nuclear double resonance.

§To whom reprint requests should be sent at the present address: Department of Physical Chemistry, University of Freiburg, Albertstrasse 21, D-79104 Freiburg, Germany.

$$H_{HF} = \sum_k \mathbf{I}_{ik}\cdot\mathbf{A}_{ik}(\Omega)\cdot\mathbf{S}_1 + \sum_l \mathbf{I}_{2l}\cdot\mathbf{A}_{2l}(\Omega)\cdot\mathbf{S}_2, \quad [5]$$

where $\mathbf{I}_{ik}$ is the spin operator of nucleus k in radical i and $\mathbf{A}_{ik}(\Omega)$ is the corresponding hyperfine tensor. a_{ik} denotes the isotropic hyperfine coupling constant,

$$a_{ik} = \frac{1}{3}\left(A_{ik}^X + A_{ik}^Y + A_{ik}^Z\right), \quad [6]$$

and A_{ik}^j, $j = X, Y, Z$, are the principal values of $\mathbf{A}_{ik}$, respectively.

The nuclei, in addition, experience Zeeman and quadrupole interactions. Thus, the last two terms of the spin Hamiltonian may be written as

$$H_{NZ} = \sum_k -\beta_n g_{1k}\mathbf{B}_0\cdot\mathbf{I}_{1k} + \sum_l -\beta_n g_{2l}\mathbf{B}_0\cdot\mathbf{I}_{2l}, \quad [7a]$$

$$H_Q = \sum_k \mathbf{I}_{1k}\cdot\mathbf{P}_{1k}(\Omega)\cdot\mathbf{I}_{1k} + \sum_l \mathbf{I}_{2l}\cdot\mathbf{P}_{2l}(\Omega)\cdot\mathbf{I}_{2l}, \quad [7b]$$

where β_n denotes the nuclear Bohr magneton. g_{1k} is the g-factor for nucleus k in radical 1 and $\mathbf{P}_{1k}(\Omega)$ is the corresponding quadrupole coupling tensor. The principal values of $\mathbf{P}(\Omega)$ are generally expressed in terms of two parameters, the quadrupole coupling constant, e^2qQ, and the asymmetry parameter, η.

Because of the explicit time dependence of $H_R(\Omega, t)$ we transform into a frame of reference, rotating with the microwave frequency ω around the static magnetic field B_0 (34). Neglect of all nonsecular terms for the electron spins (high-field approximation) renders the transformed Hamiltonian $H^r(\Omega)$ virtually time independent.

Having specified the spin Hamiltonian of the radical pair, we now employ the density operator formalism to evaluate the observable signal in a transient EPR experiment. Ignoring relaxation, the time evolution of the density matrix, $\boldsymbol{\rho}^r(t)$, can be described by the Liouville equation (35), which we solve using a finite grid point method (36, 37):

$$\frac{\partial\boldsymbol{\rho}^r(\Omega, t)}{\partial t} = (i/\hbar)[\boldsymbol{\rho}^r(\Omega, t), \mathbf{H}^r(\Omega)]. \quad [8]$$

Here $\boldsymbol{\rho}^r(\Omega, t)$ denotes the density matrix of the radical pair for a discrete orientation Ω. Formally, integration of Eq. **8** leads to

$$\boldsymbol{\rho}^r(\Omega, t) = \exp[-(i/\hbar)\mathbf{H}^r(\Omega)t]\cdot\boldsymbol{\rho}^r(\Omega, 0) \cdot\exp[(i/\hbar)\mathbf{H}^r(\Omega)t], \quad [9]$$

where $\boldsymbol{\rho}^r(\Omega, 0)$ is the initial condition of the density matrix at the time of the sudden generation of the radical pair. In native photosynthetic reaction centers the secondary radical pairs are generated in a virtually pure singlet state (12).

Evaluating the trace of $\boldsymbol{\rho}^r(t)\cdot(\mathbf{S}_1^y + \mathbf{S}_2^y)$ finally gives the observable signal as

$$M(t) = \mathrm{Tr}[\boldsymbol{\rho}^r(t)\cdot(\mathbf{S}_1^y + \mathbf{S}_2^y)], \quad [10a]$$

$$\boldsymbol{\rho}^r(t) = \int \boldsymbol{\rho}^r(\Omega, t)d\Omega, \quad [10b]$$

where $\boldsymbol{\rho}^r(\Omega, t)$ is obtained by solving Eq. **9**. The corresponding diagonalizations were accomplished by using the Housholder/QL-method. For this purpose, FORTRAN routines have been adapted from ref. 38. Spin relaxation was introduced in an *ad hoc* fashion by multiplying the time profiles with an exponential decay curve, characterized by the relaxation time T_2^{eff}. Inhomogeneous broadening was considered by convolution with a Gaussian of linewidth ΔB_0.

EXPERIMENTS

Freeze-dried, whole cells of deuterated (99.7%) and deuterated plus ^{15}N-substituted (95%) *S. lividus* cyanobacteria were suspended in deuterated Tricine buffer (uncorrected pH = 7.5). About 50 μl of the sample was used to fill a quartz tube (2 mm inner diameter) located in the symmetry axis of the microwave resonator. The temperature of the samples was controlled by using a helium flow cryostat (Oxford model CF-935) and was stable to $\pm$0.1 K.

The basic concept of the EPR experiment is similar to that described previously (21-23, 39). A modified X-band spectrometer [Bruker (Billerica, CA) model ER-200D] was used, equipped with a fast microwave preamplifier (30 decibels, 1.8-decibel noise figure) and a broad-band video amplifier (band width 200 Hz to 200 MHz). The sample was irradiated in a custom-built split-ring resonator with 2.5-ns pulses of a neodymium-doped yttrium–aluminum garnet (Nd:YAG) laser [Spectra-Physics GCR-16S, 532 nm, 5 mJ (pulse)] at a repetition rate of 10 Hz. The split-ring resonator exhibits a high filling factor at low Q (unloaded $Q \approx 500$) and provides an easy means of sample irradiation.

The time-dependent EPR signal was digitized in a transient recorder [LeCroy (Chestnut Ridge, NY) model 9450 digital oscilloscope] at a rate of 2.5 ns per 12-bit sample. The time resolution of the experimental setup is in the 10-ns range. Typically, 256 transients were accumulated at off-resonance conditions and subtracted from those on resonance to get rid of the laser background signal. The best overall view of the full data set is obtained from a two-dimensional plot of the signal intensity versus the time and magnetic field axes. Transient spectra can be extracted from this plot at any fixed time after the laser pulse as slices parallel to the magnetic field axis. Likewise, the time evolution of the transverse magnetization may be obtained for any given field as a slice along the time axis.

RESULTS AND DISCUSSION

Suspensions of deuterated and deuterated plus ^{15}N-substituted *S. lividus* were irradiated with 2.5-ns pulses from a Nd:YAG laser and the time evolution of the transverse magnetization was monitored for various static and microwave magnetic fields. Typical lineshapes, observed 200 ns after the laser pulse for deuterated (upper spectrum) and deuterated plus ^{15}N-substituted *S. lividus* (lower spectrum), are shown in Fig. 1. The spectra refer to a microwave frequency of $\omega/2\pi$ = 9.7896 GHz (X-band), a microwave field of B_1 = 0.062 mT, and T = 70 K. Note that a positive signal indicates absorptive (a) and a negative emissive (e) spin polarization. Apparently, the two lineshapes are identical within experimental error.

Fig. 2 *Left* depicts the time evolution of the transverse magnetization, measured at the middle-field absorptive maximum of the spectrum (field position B in Fig. 1). The transients refer to the deuterated ^{14}N sample, a temperature of 70 K, and two different microwave magnetic fields—i.e., B_1 = 0.049 mT (upper curve) and B_1 = 0.031 mT (lower curve). In both cases slow oscillations with frequencies of about 2 MHz can be seen. Previously, fast additional oscillations with frequencies of 5–10 MHz have been detected at this field position (21, 22). As noted above, such fast oscillations may be assigned to a zero quantum coherence between two of the four electron spin states (20–23). Because of hyperfine interactions, rapid averaging of these oscillations occurs (22). Consequently, manifestation of zero quantum coherence is restricted to a single sharp peak (dotted arrow in Fig. 2) observed immediately after the laser pulse.

Interestingly, however, the slow persisting oscillations cannot all be assigned to Torrey precessions with a frequency of

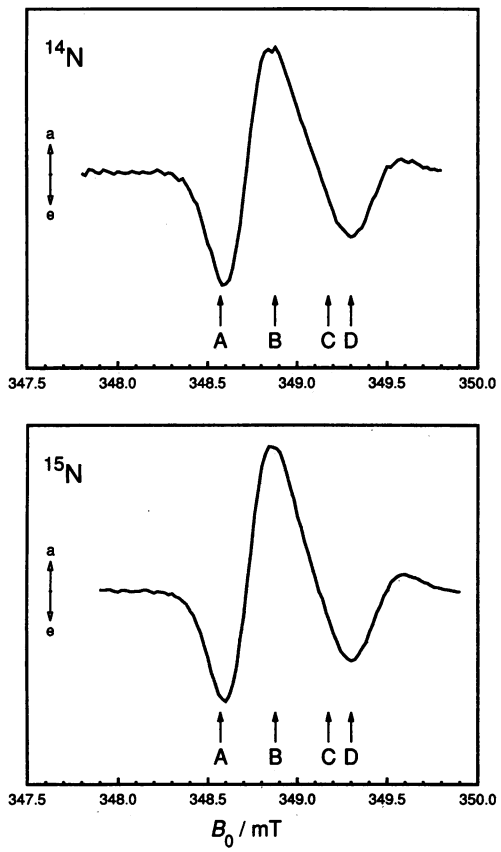

FIG. 1. Transient EPR spectra of the light-induced radical pairs $P_{700}^{+}A_1^{-}$ in PSI of deuterated (*Upper*) and deuterated plus ^{15}N-substituted *S. lividus* (*Lower*). The signal intensity was averaged in the time window 200–220 ns after laser excitation. Positive and negative signals indicate absorptive (a) and emissive (e) polarizations, respectively. Microwave frequency: $\omega/2\pi$ = 9.7896 GHz. Microwave field: B_1 = 0.062 mT. Temperature: T = 70 K. A–D indicate field positions discussed in the text.

$$\nu_{T0} \approx \frac{1}{2}(g_1 + g_2)\beta B_1/h, \qquad [11]$$

where g_i is the isotropic g-factor of radical i. Rather, there are additional modulations of the transverse magnetization. This is clearly seen in the power spectra of Fig. 2 *Right*, obtained by Fourier transformation of the time profiles (Fig. 2 *Left*). Only peaks marked with a full arrow indicate Torrey oscillations. The remaining coherences, indicative of a powder sample, exhibit frequencies between 0.2 and 3.5 MHz.

Previously, these slow oscillations of the transverse magnetization have not been observed, due to the short lifetime of $P_{700}^{+}A_1^{-}$ at T = 295 K (20–22). Apparently, cooling the sample to 70 K increases the lifetime and thus enables detection of an additional coherence phenomenon, recently reported for bacterial reaction centers (23, 24). It is tempting to assign these slow oscillations to nuclear quantum beats, associated with the nonadiabatic change of the spin Hamiltonian at the instant of the laser pulse. Since the initial nuclear spin configurations are not eigenstates of the radical pair Hamiltonian, the light pulse induces a coherent time evolution of the nuclear spin system (18). This nuclear coherence could then be transferred to observable electron coherence by means of the continuous microwave magnetic field. In this case, the frequencies of the oscillations would be equal to differences between nuclear spin levels and thus correspond to electron nuclear double resonance (ENDOR) frequencies.

To validate these ideas, additional experiments have been carried out. In Fig. 3 we compare power spectra from the deuterated ^{14}N sample (*Left*) and the deuterated ^{15}N sample (*Right*), measured at two different static magnetic fields (A and C in Fig. 1). All spectra refer to the same microwave field of B_1 = 0.062 mT. Apparently, at this high B_1 field Torrey oscillations are difficult to detect (full arrows in Fig. 3). Furthermore, the modulation pattern varies across the powder lineshape, as expected for a weakly coupled pair of different radicals. Interestingly, the same pattern is observed at position A for both the deuterated ^{14}N and deuterated ^{15}N samples. Thus, nitrogens are not the source of modulation at this field position. Note the intense peak at 2.3 MHz, which corresponds closely to the free deuteron precession in the static field of 348.9 mT, thus indicating a matrix ENDOR line.

At field position C the observed power spectra are different for the different samples. The change in the modulation pattern indicates that the modulations are due to nitrogen nuclei, ^{14}N and ^{15}N. From Fig. 3 we determine modulation frequencies of 2.0 and 2.6 MHz for the ^{14}N sample and of 1.9 and 2.3 MHz for the ^{15}N sample. These values are in line with values assigned to ^{14}N and ^{15}N ENDOR frequencies in PSI preparations (40–43). We therefore conclude that nuclear quantum beats have been detected in the transverse electron

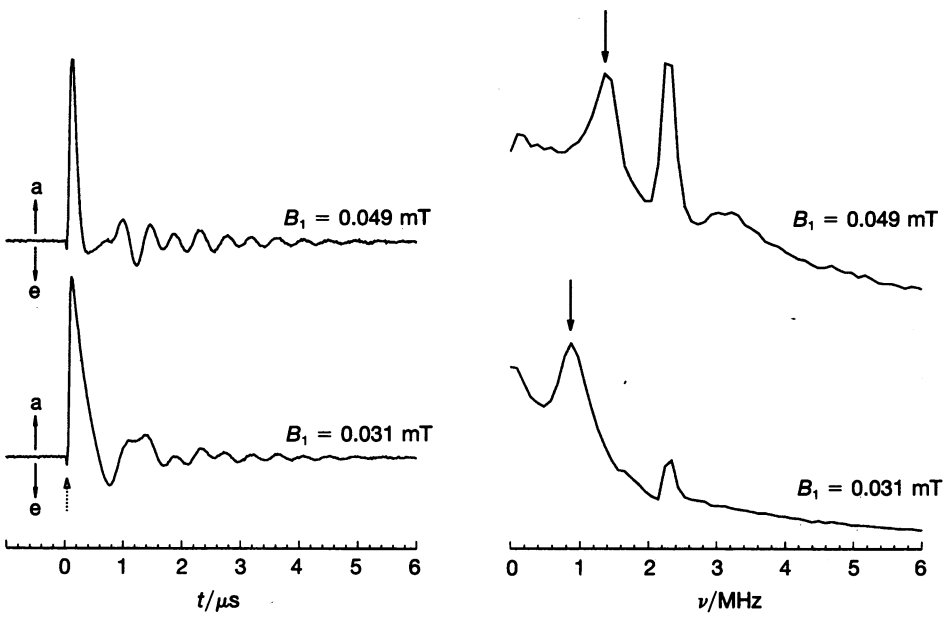

FIG. 2. Time evolution of the transverse magnetization of the light-induced radical pairs $P_{700}^{+}A_1^{-}$ in PSI of deuterated *S. lividus*. The transients were taken at the middle-field absorptive maximum of the spectrum (field position B in Fig. 1) and refer to two different microwave magnetic fields—i.e., B_1 = 0.049 mT (upper curves) and B_1 = 0.031 mT (lower curves). Microwave frequency: $\omega/2\pi$ = 9.7896 GHz. Temperature: T = 70 K. (*Left*) Time profiles. Zero quantum precessions are indicated by a dotted arrow. (*Right*) Power spectra. Torrey oscillations are indicated by a full arrow.

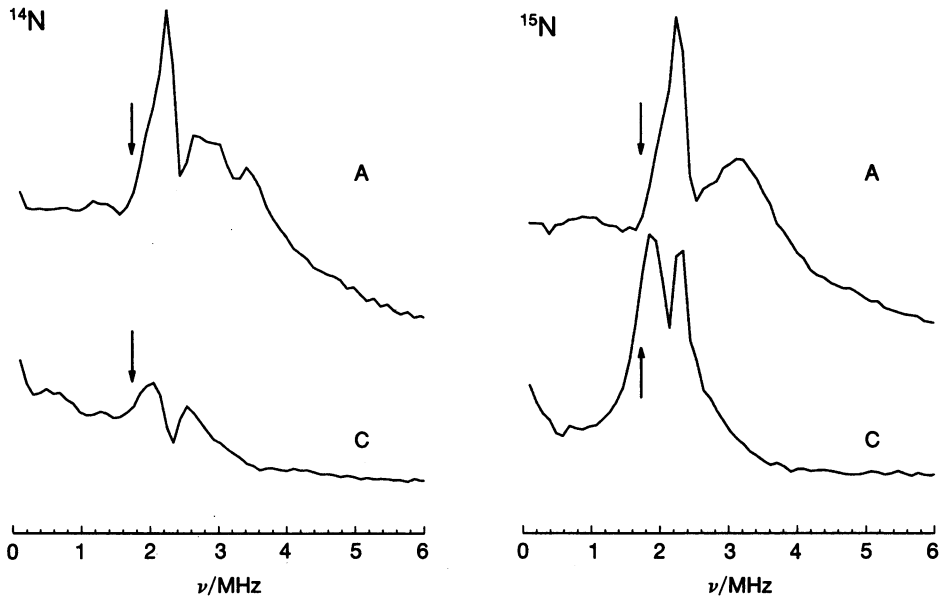

FIG. 3. Fourier transform of experimental EPR time profiles of the light-induced radical pairs $P_{700}^{+}A_1^{-}$ in PSI of deuterated (*Left*) and deuterated plus ^{15}N-substituted *S. lividus* (*Right*). The power spectra were taken at the low-field emissive maximum (field position A in Fig. 1) and high-field emissive maximum (field position C in Fig. 1). Arrows indicate the calculated position of the Torrey oscillations. Microwave frequency: $\omega/2\pi$ = 9.7896 GHz. Microwave field: B_1 = 0.062 mT. Temperature: T = 70 K. Upper curves: power spectra at field position A. Lower curves: power spectra at field position C.

magnetization of $P_{700}^{+}A_1^{-}$. This result confirms the interpretations of recent observations in bacterial reaction centers (23, 24).

Detection of nuclear quantum beats is intimately related to other coherence phenomena in EPR such as coherent Raman beats (44, 45) and electron spin echo envelope modulation (ESEEM) (46, 47). Note, however, that in the present case nuclear spin coherence is generated simply by a short laser pulse and does not require preparation by pulsed microwaves (44–47). This represents a unique feature of rapid charge separation such as in photosynthesis. It appears that light generation of nuclear coherence provides an alternative to standard ESEEM schemes and because of the longer decay times is distinguished by a greater spectral resolution (40–43).

To check the above assignments, model calculations were performed employing the EPR approach, outlined in *Theory*. For computational simplicity, nuclear spin interactions were restricted to one ^{15}N nucleus in P_{700}^{+} and five deuterons in A_1^{-}. In addition, pseudosecular hyperfine and nuclear quadrupole interactions for the deuterons have been neglected in the calculations. Furthermore, the ^{15}N coupling tensor was assumed to be collinear with the g-tensor of P_{700}^{+}. The parameters used to calculate the nuclear quantum beats are summarized in Table 1.

The g-tensor components of P_{700}^{+} and A_1^{-} were adapted from high-field EPR studies of deuterated PSI preparations (48) and model compounds (50). The listed spin–spin coupling parameters are estimates based on the low-resolution x-ray structure (26). The geometry of $P_{700}^{+}A_1^{-}$ was determined from the B_0 dependence of the early oscillations (22). The listed Euler angles relate the principal axis system of the respective magnetic tensor and the molecular reference system [g-tensor of A_1^{-} (49)].

Typically, 5000 grid points, regularly spaced over the surface of a sphere, were employed to simulate the static distribution of the radical pair with respect to the laboratory frame. Fig. 4 shows calculated time profiles (*Upper*) and corresponding power spectra (*Lower*), evaluated at field position D (see Fig. 1) for a microwave magnetic field of B_1 = 0.1 mT. The magnetic field parameters were chosen to optimize the modulation depth. Three different frequencies can be distinguished. The intense peak at 2.8 MHz (full arrow) corresponds to Torrey oscillations. In contrast, the broad peak at 13 MHz (dotted arrow), independent of B_1, can be assigned to a zero quantum coherence between two of the four electron spin states (22). Notably, the remaining peak at 2.4 MHz disappears if ^{15}N pseudosecular terms are neglected in the calculations (dotted curves in Fig. 4). We therefore conclude that assignment of this peak to ^{15}N nuclear modulations is correct.

At present accurate values for the ^{15}N hyperfine interactions in P_{700}^{+} do not exist. Even the total number of ^{15}N nuclei involved in coupling is not unambiguously known. Additional studies of light-induced nuclear quantum beats may provide the desired information. From the results of initial studies along these lines, involving protonated ^{15}N-enriched PSI preparations, we expect detailed information on the electronic structure of P_{700}^{+}, which is essential for a better understanding of the primary events of plant photosynthesis.

Table 1. Parameters used in model calculations for the light-induced radical pairs $P_{700}^{+}A_1^{-}$ in deuterated plant PSI

g-Tensor components P_{700}^{+}*	g-Tensor orientation P_{700}^{+}†	g-Tensor components A_1^{-}‡	Spin–spin coupling parameters§	Dipolar tensor orientation†	Hyperfine tensor components P_{700}^{+}¶	Hyperfine tensor components A_1^{-}‖	Relaxation parameters**
g_1^X = 2.00304	ϕ_1 = −15°	g_2^X = 2.00564	J = 0	ϕ_D arbitrary	A_{1N}^X = 0.060 mT	A_{2D}^X = 0.063 mT	T_2^{eff} = 2 μs
g_1^Y = 2.00262	θ_1 = 28°	g_2^Y = 2.00494	D = −0.12 mT	θ_D = 58°	A_{1N}^Y = 0.060 mT	A_{2D}^Y = 0.063 mT	ΔB_0 = 0.175 mT
g_1^Z = 2.00232	ψ_1 = 27°	g_2^Z = 2.00217	E = 0	ψ_D = −1°	A_{1N}^Z = 0.150 mT	A_{2D}^Z = 0.063 mT	

*Data from ref. 48.
†The Euler angles Ω_i relate the principal axis system of the respective magnetic tensor (g-tensor of P_{700}^{+}, dipolar coupling tensor, nitrogen hyperfine tensor) and the molecular reference system [g-tensor of A_1^{-} (49)]. Data from ref. 22.
‡Adapted from ref. 50.
§Estimated on the basis of a low-resolution x-ray structure (26).
¶Data from ref. 43.
‖Adapted from ref. 22.
**Spin relaxation is considered by multiplying the time profiles by an exponential decay curve, characterized by the relaxation time T_2^{eff}. Inhomogeneous broadening is considered by convolution with a Gaussian of linewidth ΔB_0 = 0.175 mT (39).

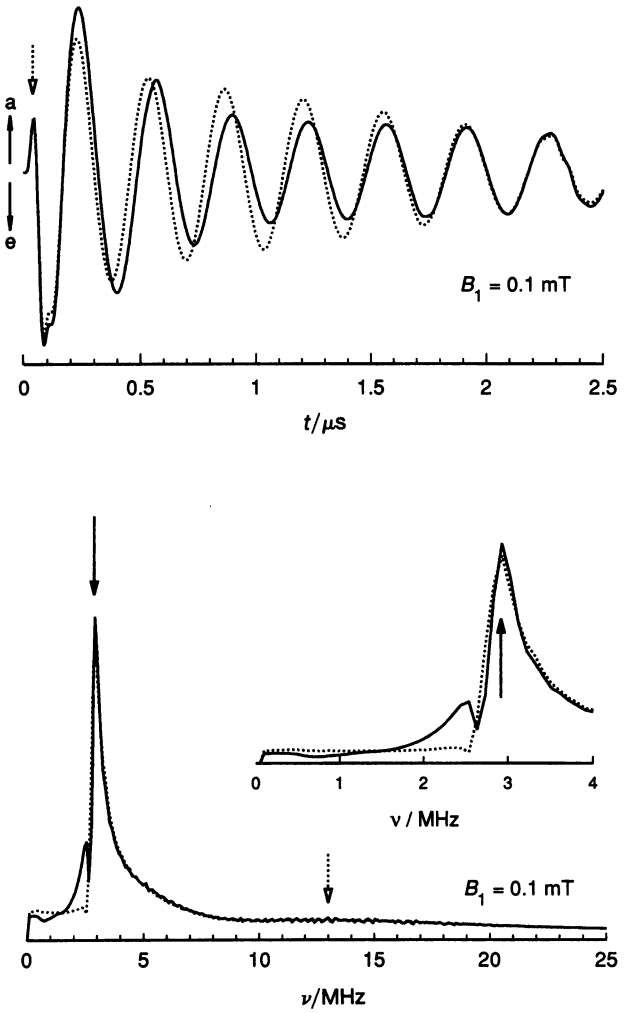

FIG. 4. Calculated time profiles (*Upper*) and corresponding power spectra (*Lower*) of the light-induced radical pairs $P_{700}^{+}A_1^{-}$ in PSI. The transients were evaluated at field position D (see Fig. 1), using the parameters of Table 1. Microwave frequency: $\omega/2\pi$ = 9.7896 GHz. Microwave field: B_1 = 0.1 mT. Torrey oscillations are indicated by a full arrow. Zero quantum precessions are denoted by a dotted arrow. The dotted curves represent model calculations in which ^{15}N pseudo-secular terms have been neglected.

Financial support by the U.S. Department of Energy, Office of Basic Energy Sciences, Division of Chemical Sciences (Contract W-31-109-ENG-38) and by the Deutsche Forschungsgemeinschaft is gratefully acknowledged. J.R.N. acknowledges support from the Humboldt Foundation.

1. Thurnauer, M. C. & Norris, J. R. (1980) *Chem. Phys. Lett.* **76,** 557–561.
2. Thurnauer, M. C. & Meisel, D. (1983) *J. Am. Chem. Soc.* **105,** 3729–3731.
3. Closs, G. L., Forbes, M. D. E. & Norris, J. R. (1987) *J. Phys. Chem.* **91,** 3592–3599.
4. Buckley, C. D., Hunter, D. A., Hore, P. J. & MacLauchlan, K. A. (1987) *Chem. Phys. Lett.* **135,** 307–312.
5. Hore, P. J., Hunter, D. A., McKie, C. D. & Hoff, A. J. (1987) *Chem. Phys. Lett.* **137,** 495–500.
6. Stehlik, D., Bock, C. H. & Petersen, J. (1989) *J. Phys. Chem.* **93,** 1612–1619.
7. Hore, P. J. (1989) in *Advanced EPR: Applications in Biology and Biochemistry*, ed. Hoff, A. J. (Elsevier, Amsterdam), pp. 405–440.
8. Stehlik, D., Bock, C. H. & Thurnauer, M. C. (1989) in *Advanced EPR: Applications in Biology and Biochemistry*, ed. Hoff, A. J. (Elsevier, Amsterdam), pp. 371–403.
9. Feezel, L. L., Gast, P., Smith, U. H. & Thurnauer, M. C. (1989) *Biochim. Biophys. Acta* **974,** 149–155.
10. Morris, A. L., Norris, J. R. & Thurnauer, M. C. (1990) in *Reaction Centers of Photosynthetic Bacteria*, Springer Series in Biophysics, ed. Michel-Beyerle, M.-E. (Springer, Berlin), Vol. 6, pp. 423–435.
11. Norris, J. R., Morris, A. L., Thurnauer, M. C. & Tang, J. (1990) *J. Chem. Phys.* **92,** 4239–4249.
12. Synder, S. W., Morris, A. L., Bondenson, S. R., Norris, J. R. & Thurnauer, M. C. (1993) *J. Am. Chem. Soc.* **115,** 3774–3775.
13. Proskuryakov, I. I., Klenina, I. B., Shkuropatov, A. Ya., Shkuropatova, V. A. & Shuvalov, V. A. (1993) *Biochim. Biophys. Acta* **1142,** 207–210.
14. Snyder, S. W. & Thurnauer, M. C. (1993) in *The Photosynthetic Reaction Center*, eds. Deisenhofer, J. & Norris, J. R. (Academic, New York), pp. 285–330.
15. Salikhov, K. M., Bock, C. H. & Stehlik, D. (1990) *J. Appl. Magn. Reson.* **1,** 195–211.
16. Bittl, R. & Kothe, G. (1991) *Chem. Phys. Lett.* **177,** 547–553.
17. Wang, Z., Tang, J. & Norris, J. R. (1992) *J. Magn. Reson.* **97,** 322–334.
18. Salikhov, K. M. (1993) *Chem. Phys. Lett.* **201,** 261–264.
19. Zwanenburg, G. & Hore, P. J. (1993) *Chem. Phys. Lett.* **203,** 65–74.
20. Kothe, G., Weber, S., Bittl, R., Norris, J. R., Snyder, S. S., Tang, J., Thurnauer, M. C., Morris, A. L., Rustandi, R. R. & Wang, Z. (1991) in *Spin Chemistry*, ed. I'Haya, Y. J. (The Oji International Conference on Spin Chemistry, Tokyo), pp. 420–434.
21. Kothe, G., Weber, S., Bittl, R., Ohmes, E., Thurnauer, M. C. & Norris, J. R. (1991) *Chem. Phys. Lett.* **186,** 474–480.
22. Kothe, G., Weber, S., Ohmes, E., Thurnauer, M. C. & Norris, J. R. (1994) *J. Phys. Chem.* **98,** 2706–2712.
23. Kothe, G., Weber, S., Ohmes, E., Thurnauer, M. C. & Norris, J. R. (1994) *J. Am. Chem. Soc.*, **116,** 7729–7734.
24. Bittl, R., van der Est, A., Kamlowski, A., Lubitz, W. & Stehlik, D. (1994) *Chem. Phys. Lett.* **226,** 349–358.
25. Golbeck, J. H. & Bryant, D. A. (1992) *Curr. Topics Bioenerg.* **16,** 83–177.
26. Krauss, N., Hinrichs, W., Witt, I., Fromme, P., Pritzkow, W., Dauter, Z., Betzel, C., Wilson, K. S., Witt, H. & Saenger, W. (1993) *Nature (London)* **361,** 326–331.
27. Norris, J. R., Uphaus, R. A. Crespi, H. L. & Katz, J. J. (1971) *Proc. Natl. Acad. Sci. USA* **68,** 625–628.
28. Sieckmann, I., Brettel, K., Bock, C., van der Est, A. & Stehlik, D. (1993) *Biochemistry* **32,** 4842–4847.
29. Snyder, S. W., Rustandi, R. R., Biggins, J., Norris, J. R. & Thurnauer, M. C. (1991) *Proc. Natl. Acad. Sci. USA* **88,** 9895–9896.
30. Thurnauer, M. C., Bowman, M. K. & Norris, J. R. (1979) *FEBS Lett.* **100,** 309–312.
31. McIntosh, A. R., Manikowski, H., Wong, S. K., Taylor, C. P. S. & Bolton, J. R. (1979) *Biochem. Biophys. Res. Commun.* **87,** 605–612.
32. Rustandi, R. R., Snyder, S. W., Feezel, L. L., Michalski, T. J., Norris, J. R., Thurnauer, M. C. & Biggins, J. (1990) *Biochemistry* **29,** 8030–8032.
33. Reitz, D. C. & Weissman. S. I. (1960) *J. Chem. Phys.* **33,** 700–704.
34. Redfield, A. G. (1955) *Phys. Rev.* **98,** 1787–1801.
35. Slichter, C. P. (1992) *Principles of Magnetic Resonance* (Springer, Berlin), pp. 158–159.
36. Norris, J. R. & Weissman, S. I. (1969) *J. Phys. Chem.* **73,** 3119–3124.
37. Kothe, G. (1977) *Mol. Phys.* **33,** 147–158.
38. Press, W. H., Flannery, B. P., Teukolsky, S. A. & Vetterling, W. T. (1989) *Numerical Recipes: The Art of Scientific Computing* (Cambridge Univ. Press, Cambridge, U.K.), Chapt. 11, pp. 335–365.
39. Münzenmaier, A., Rösch, N., Weber, S., Feller, C., Ohmes, E. & Kothe, G. (1992) *J. Phys. Chem.* **96,** 10645–10653.
40. Dikanov, S. A., Astashkin, A. V., Tsvetkov, Yu. D. & Goldfield, M. G. (1983) *Chem. Phys. Lett.* **101,** 206–210.
41. Thurnauer, M. C. & Clark, C. (1984) *Photochem. Photobiol.* **40,** 381–386.
42. Davis, I. H., Heathcote, P., MacLachlan, D. J. & Evans, M. C. W. (1993) *Biochim. Biophys. Acta* **1143,** 183–189.
43. Käss, H., Bittersmann-Weidlich, E., Andréasson, L.-E., Bönigk, B. & Lubitz, W. (1995) *Chem. Phys.* **194,** 419–432.
44. Bowman, M. K., Massoth, R. J. & Yannoni, C. S. (1992) in *Pulsed Magnetic Resonance: NMR, EPR and Optics*, ed. Bagguley, D. M. S. (Clarendon, Oxford), pp. 423–445.
45. Bowman, M. K. (1992) *Israel J. Chem.* **32,** 31–40.
46. Rowan, L. G., Hahn, E. L. & Mims, W. B. (1965) *Phys. Rev. A* **137,** 61–71.
47. Mims, W. B. (1972) *Phys. Rev. B* **5,** 2409–2419.
48. Prisner, T. F., McDermott, A. E., Un, S., Norris, J. R., Thurnauer, M. C. & Griffin, R. G. (1993) *Proc. Natl. Acad. Sci. USA* **90,** 9485–9488.
49. Hales, B. F. (1975) *J. Am. Chem. Soc.* **97,** 5993–5997.
50. Burghaus, O., Plato, M., Rohrer, M., Möbius, K., McMillian, F. & Lubitz, W. (1993) *J. Phys. Chem.* **97,** 7639–7647.